Regulation of the hypertonic stress response by the 3' mRNA cleavage and polyadenylation complex

Sarel J. Urso[1,2], Anson Sathaseevan[3], W. Brent Derry[3], and Todd Lamitina*,[1,2,4]

[1]Graduate Program in Cell Biology and Molecular Physiology, University of Pittsburgh Medical Center

[2] Department of Cell Biology, University of Pittsburgh School of Medicine

[3] Developmental and Stem Cell Biology Program, Peter Gilgan Centre for Research and Learning, The Hospital for Sick Children, Toronto, ON M5G 0A4, Canada.

[4] Division of Child Neurology, Department of Pediatrics, Children's Hospital of Pittsburgh, University of Pittsburgh Medical Center, Pittsburgh, PA, USA

*Address correspondence to Todd Lamitina, Ph.D., Children's Hospital of Pittsburgh of the University of Pittsburgh Medical Center, Departments of Pediatrics and Cell Biology, 4401 Penn Avenue, Rangos 7122, Pittsburgh, PA 15224, phone - (412) 692-9437; fax – (412) 641-1844; email - stl52@pitt.edu

Abstract

Maintenance of osmotic homeostasis is one of the most aggressively defended homeostatic setpoints in physiology. One major mechanism of osmotic homeostasis involves the upregulation of proteins that catalyze the accumulation of solutes called organic osmolytes. To better understand how osmolyte accumulation proteins are regulated, we conducted forward genetic screen in *C. elegans* for mutants with no induction of osmolyte biosynthesis gene expression (Nio mutants). *nio-3* mutants encoded a missense mutation in *cpf-2*/CstF64 while *nio-7* mutants encoded a missense mutation in *symk-1*/Symplekin. Both *cpf-2* and *symk-1* are nuclear components of the highly conserved 3' mRNA cleavage and polyadenylation complex. *cpf-2* and *symk-1* block the hypertonic induction of *gpdh-1* and other osmotically induced mRNAs, suggesting they act at the transcriptional level. We generated a functional auxin-inducible degron (AID) allele for *symk-1* and found that acute, post-developmental degradation in the intestine and hypodermis was sufficient to cause the Nio phenotype. *symk-1* and *cpf-2* exhibit genetic interactions that strongly suggest they function through alterations in 3' mRNA cleavage and/or alternative polyadenylation. Consistent with this hypothesis, we find that inhibition of several other components of the mRNA cleavage complex also cause a Nio phenotype. *cpf-2* and *symk-1* specifically affect the osmotic stress response since heat shock-induced upregulation of a *hsp-16.2::GFP* reporter is normal in these mutants. Our data suggest a model in which alternative polyadenylation of one or more mRNAs is essential to regulate the hypertonic stress response.

Introduction

mRNA processing plays a key role in the response to diverse types of environmental stress. For example, post-transcriptional splicing of the *xbp-1* mRNA by activated IRE1 endonuclease is the key step in activation of the endoplasmic reticulum (ER) stress response (CALFON *et al.* 2002). In the DNA damage response, localized mRNA splicing plays a key role in the active repair of double strand breaks (SHANBHAG *et al.* 2010; PEDERIVA *et al.* 2016). Recently, 3' mRNA cleavage components from transcriptionally active genomic loci were found to undergo hyperosmotic stress induced phase separation, which was associated with a global impairment of transcriptional termination (JALIHAL *et al.* 2020). Whether or not 3' mRNA cleavage or other types of mRNA processing play a more direct functional role in the regulation of the hyperosmotic stress response is unknown.

In eukaryotes, the 3' ends of ~30-60% of all mRNAs are cleaved and polyadenylated at more than one polyadenylation site (PAS), which results in mRNAs with different 3' ends (STEBER *et al.* 2019; YUAN *et al.* 2021). Much like alternative splicing, alternative polydenylation (APA) also leads to the diversification of mRNA transcripts through two distinct mechanisms. First, 3' UTR APA gives rise to mRNAs with different length 3' UTRs, which can provide isoform specific binding sites for mRNA regulators such as micro RNAs (miRNAs) and RNA binding proteins (MAYR AND BARTEL 2009). Second, upstream region APA (UR-APA) can include alternative exons that, when translated, give rise to proteins with unique sequences and/or domains (ALT *et al.* 1980). The 3' mRNA end processing complex is composed of ~85 proteins that regulate mRNA cleavage, polyadenylation, and APA (SHI *et al.* 2009). Biochemical and structural features of the core complex of ~20 protein are relatively well described (PANCEVAC *et al.* 2010; CLERICI *et al.* 2017; CLERICI *et al.* 2018) and new sequencing

and bioinformatics approaches are enabling the identification of mRNA targets of APA (HA *et al.* 2018; WANG *et al.* 2018). While APA is associated with aspects of cellular physiology, such as cellular stress responses (CHANG *et al.* 2018; ZHENG *et al.* 2018), the physiological roles of 3' mRNA cleavage/APA are poorly understood, largely because genetic null alleles of most 3' mRNA cleavage components are lethal, although some important exceptions do exist (SUBRAMANIAN *et al.* 2021).

In *C. elegans*, hypertonic stress activates a gene expression program that restores cell volume and protects against hypertonicity-induced macromolecular damage (ROHLFING *et al.* 2010). Like all cells and organisms, *C. elegans* uses solutes called organic osmolytes to restore volume and provide protection (LAMITINA *et al.* 2004; LAMITINA *et al.* 2006; BURKEWITZ *et al.* 2012). The major *C. elegans* osmolyte is glycerol, which is rapidly accumulated following exposure to hypertonicity, in part through the upregulation of the glycerol-3-phosphate dehydrogenase *gpdh-1* (LAMITINA *et al.* 2004). Genetic screens for regulators of *gpdh-1* expression have identified many positive and negative regulators of this stress response pathway (LAMITINA *et al.* 2006; WHEELER AND THOMAS 2006; ROHLFING *et al.* 2011; DODD *et al.* 2018; URSO *et al.* 2020; WIMBERLY AND CHOE 2022). However, it is not known whether components of the 3' mRNA cleavage complex play a functional role in the regulation of the hypertonic stress response.

Using unbiased forward genetic screening for mutants that exhibit no induction of *gpdh-1* expression in response to hypertonicity, we identified viable hypomorphic alleles of two 3' mRNA cleavage complex genes, *cpf-2* and *symk-1*. *cpf-2* and *symk-1* physiologically regulate the transcriptional induction of multiple hypertonicity induced mRNAs through their activity in the hypodermis and intestine. CPF-2 and SYMK-1 proteins co-localize within the nucleus of all cells and form subnuclear puncta in

response to hypertonicity. Both *symk-1* and *cpf-2* mutants do not significantly alter general mRNA polyadenylation but instead exhibit phenotypes consistent with inhibition of APA. Consistent with this hypothesis, inhibition of several other 3' mRNA cleavage complex genes also blocks hypertonic induction of *gpdh-1* transcription. *cpf-2* and *symk-1* are not required for the transcriptional induction of a heat shock inducible GFP reporter, suggesting that their roles in regulating stress response pathways may be specific. Our findings reveal a physiological role for the 3' mRNA cleavage complex complex in the hypertonic stress response and provide new genetic tools that should facilitate the *in vivo* study of this essential mRNA regulatory mechanism in developmental and tissue-specific contexts.

Results

In a forward genetic screen for mutants with no induction of the osmolyte biosynthetic transcriptional reporter *gpdh-1p::gfp* reporter (Nio muants), we identified *nio-3(dr16)* and *nio-3(dr23)*. Mapping, complementation testing, and whole genome sequencing revealed that *dr16* caused a G42E missense mutation in the *cpf-2* gene while *dr23* caused a R580W missense mutation in the *symk-1* gene (Fig. 1A). Both alleles were genetically recessive and segregated Nio animals from heterozygous hermaphrodites close to expected single gene Mendelian ratios (*dr16* – 24/111, 21.6%; *dr23* – 22/145, 15.2%). *cpf-2* and *symk-1* encode two proteins that are core components of the 3' mRNA cleavage and polyadenylation complex and are known to interact in mammalian cells (RUEPP *et al.* 2011). This complex recognizes polyadenylation signals in the mRNA and directs mRNA cleavage and transcriptional termination through a multi-subunit protein complex (SHI *et al.* 2009). Several additional experiments show that these non-null mutations in *cpf-2* and *symk-1* are the basis for the Nio phenotype. First, post-embryonic RNAi of both *cpf-2* and *symk-1* also caused a Nio phenotype (Fig S1). Second, extrachromosomal arrays carrying either fosmids or genomic DNA PCR products encompassing either the *cpf-2* and *symk-1* loci rescue *dr16* and *dr23* accordingly (Fig. S2). Third, CRISPR engineered alleles of *dr16* and *dr23* that recreated each missense mutation in a non-mutagenized *drIs4* background also blocked hypertonic induction of *gpdh-1p::GFP* (Fig. 1B,C) and eliminated the ability to adapt to normally lethal hypertonic environments (Fig. 1D). Notably, null or strong loss of function alleles of both *cpf-2* and *symk-1* are embryonic/larval lethal (STEBER *et al.* 2019) whereas the Nio alleles are viable and fertile under isotonic conditions. Taken together, these data show that *nio-3(dr16)* and *nio-7(dr23)* are caused by non-null hypomorphic alleles in *cpf-2* and *symk-1*.

The Nio screen utilized the *drIs4* reporter strain to identify mutants with defective transcriptional responses to hypertonic stress. To determine if these alleles also affected endogenous mRNAs, we performed qPCR on several genes previously shown to be upregulated by hypertonicity (ROHLFING *et al.* 2010). Hypertonic upregulation of endogenous *gpdh-1* mRNA, as well as another hypertonicity upregulated gene *hmit-1.1* and the transgene derived *gfp* mRNA, was strongly attenuated in both *cpf-2(dr99)* and *symk-1(dr88)* (Fig. 2). However, upregulation of *nlp-29*, an antimicrobial peptide previously shown to be induced by infection, wounding, and hypertonicity (PUJOL *et al.* 2008), continued to be upregulated to wild type levels in *cpf-2(dr99)* and *symk-1(dr88)*. Therefore *cpf-2* and *symk-1* are required to upregulate some but not all hypertonicity responsive mRNAs.

gpdh-1 is upregulated by hypertonic stress in the intestine and the hypodermis (LAMITINA *et al.* 2004; LAMITINA *et al.* 2006). If *cpf-2* and *symk-1* function cell autonomously, then they should also be required in the intestine and hypodermis to upregulate *gpdh-1* in response to hypertonicity. To test this hypothesis, we generated auxin-inducible degradation (AID*) alleles for both *cpf-2* and *symk-1* using CRISPR/Cas9 methods. The *AID*-GFP-cpf-2* allele was sick and exhibited low fecundity, suggesting the presence of non-specific *cpf-2* degradation and was not studied further. However, the *symk-1::GFP::AID** allele exhibited qualitatively normal growth and fertility in the absence of auxin, suggesting this allele is functional. We generated homozygous *symk-1::GFP::AID** alleles in genetic backgrounds expressing the TIR1 E3 ligase in all cells, hypodermis, intestine, or hypodermis and intestine (ASHLEY *et al.* 2021). While *symk-1::GFP::AID** animals expressing global TIR1 robustly expressed nuclear GFP in all somatic and germline cells in the absence of auxin, exposure of animals to 0.5mM auxin led to loss of the GFP signal in all tissues within 3-4

154 hours (Fig. S3). Additionally, 100% of the progeny derived from L4 animals exposed to
155 0.5mM auxin paired with global expression of TIR1 were embryonic or larval lethal,
156 suggesting that auxin-induced depletion of *symk-1* mimics the *symk-1* null phenotype.
157 Next, we examined induction of the *gpdh-1p::GFP* reporter in each TIR1 strain in
158 the absence of auxin. GFP expression was induced in the intestine and hypodermis to
159 similar levels as wild type (Fig. S4). When animals were exposed to auxin starting as
160 L1s, hypertonic induction of GFP was inhibited in the global TIR1 strain as much as in
161 the *symk-1(dr88)* allele (Fig. 3A,B). Hypodermal depletion of *symk-1* led to an almost
162 complete inhibition of GFP induction by hypertonicity, while intestinal depletion of *symk-1*
163 had a minor effect. However, simultaneous depletion of *symk-1* in both the intestine and
164 hypodermis resulted in a complete block in hypertonicity *induced gpdh-1::GFP*
165 expression. We next utilized the *symk-1 AID** allele and hypodermal/intestinal TIR1 to
166 examine the temporal requirements for *symk-1* in the activation of *gpdh-1*. Exposure to
167 auxin for four hours in Day 1 adult animals immediately prior to exposure to hypertonicity
168 was sufficient to block *gpdh-1p::GFP* expression (Fig. 3C). Taken together, these data
169 show that *symk-1* functions cell autonomously in the hypodermis and intestine to
170 regulate hypertonic *gpdh-1* induction. Additionally, they show that *symk-1* has a post-
171 developmental physiological role in this process.
172 If *cpf-2* and *symk-1* interact within the 3' mRNA cleavage complex in *C. elegans*
173 as they do in mammalian cells (RUEPP *et al.* 2011), we predicted that they should exhibit
174 spatial co-localization. Indeed, GFP and RFP alleles of endogenous *cpf-2* and *symk-1*,
175 respectively, showed that both proteins are expressed ubiquitously, exhibit co-
176 localization in the nucleoplasm, and are excluded from the nucleolus (Fig. 4). Following
177 exposure to hypertonicity, both proteins formed subnuclear puncta that exhibited
178 complete co-localization. In the same screen that isolated *cpf-2* and *symk-1*, we also

identified mutations in the O-GlcNAc transferase homolog *ogt-1*, suggesting that these three proteins could be components of the same complex that regulates the hypertonic stress response. However, our data were inconsistent with this model. We found that that the CPF-2 and SYMK-1 puncta were distinct from previously reported OGT-1 puncta induced by hypertonic stress (Fig S5) (URSO *et al.* 2020). Hypertonicity induced CPF-2/SYMK-1 puncta were most apparent in the hypodermis and to a lesser extent in the intestine, while no puncta were observed in germline nuclei (Fig. 4). Introduction of the Nio allele G42E into *TagRFP-cpf-2* did not alter CPF-2 protein abundance, nuclear localization, puncta formation, or co-localization with SYMK-1.

The 3' mRNA cleavage and polyadenylation complex is required for recognition of DNA-encoded polyadenylation signal sequences, transcriptional termination via mRNA cleavage, and mRNA polyadenylation. Mutation of *cpf-2* and *symk-1* could cause a Nio phenotype by disrupting these or other processes. Three pieces of data suggest that the Nio alleles do not disrupt global mRNA cleavage and/or polyadenylation at a significant level. First, total RNA levels are not decreased in either *cpf-2(dr99)* or *symk-1(dr88)* (Fig. S6). Second, polyA patterns and lengths for several mRNAs are not altered in either *cpf-2(dr99)* or *symk-1(dr88)* (Fig. S7). Third, induction of a heat shock inducible *hsp-16p::GFP* reporter, which shares the same *unc-54* 3'UTR and polyA signal as the *gpdh-1p::GFP* reporter, is induced to wild type levels in *cpf-2(dr99)* and *symk-1(dr88)* (Fig. S8). Therefore, inhibition of *cpf-2* and *symk-1* does not generally block mRNA cleavage and polyadenylation.

To test if the Nio mutants alter transcriptional termination and/or recognition of specific polyA signal sequences, we asked if they could suppress phenotypes associated with either *lin-15(n765ts)* or *kin-20(ox423)*. Previous studies demonstrated that inhibition of some core components of the 3' mRNA cleavage complex suppresses

these alleles specifically due to alterations in the ability of the complex to appropriately recognize DNA encoded alternative polyadenylation signal sequences (CUI *et al.* 2008; LABELLA *et al.* 2020). We found that the Nio allele of *cpf-2* completely suppressed the multivulval phenotype *of lin-15(n765)* (Fig. 5). Additionally, *symk-1* and *cpf-2* Nio alleles both suppressed the motility defects associated with the *kin-20* LOF mutation as well or better than the previously identified *kin-20* suppressor *cpsf-4(ox645)* (Fig. 5). Together, these data show that *cpf-2* and *symk-1* Nio alleles both act to inhibit 3' mRNA cleavage and can disrupt alternative polyadenylation for these specific transcripts.

To further test this hypothesis, we examined if the Nio phenotype was only caused by disruption of *cpf-2* and *symk-1* or if inhibition of other genes in the 3' mRNA cleavage complex could also cause a Nio phenotype. 16/17 genes in the 3' mRNA cleavage complex have clear orthologs in *C. elegans (STEBER et al. 2019)*. We obtained RNAi clones for 12/17 genes and performed post-developmental feeding based RNAi in the *gpdh-1p::GFP* reporter strain. Following exposure to hypertonic stress, knockdown of *suf-1*, *cpsf-2*, *cpsf-4*, and *rbpl-1*, in addition to *cpf-2* and *symk-1* (6/12 tested), gave rise to a Nio phenotype (Fig. 6). Therefore, the Nio phenotype is not restricted to disruption of *cpf-2* and *symk-1* specifically but is caused by inhibition of multiple genes in the 3' mRNA cleavage complex. Taken together, these data are consistent with a model in which inhibition of *cpf-2* and *symk-1* prevent hypertonic induction of *gpdh-1* due to the inability to recognize appropriate polyA signal sequences in a gene(s) required for activation of the hypertonic stress response.

Discussion

Phenotypes associated with loss of components of the 3' mRNA cleavage complex, particularly at the organismal level, are poorly understood due to the fact that loss of function mutants in most members of this complex are lethal (STEBER *et al.* 2019). One recent exception to this is in *C. elegans*, where unbiased genetic screens can isolate non-null hypomorphic alleles of genes whose null phenotype is lethal. For example, APA of the *unc-44*/ankyrin mRNA utilizes a distal polyA site in both GABA neurons and hypodermal cells to produce 'Giant' ankyrin (CHEN *et al.* 2017; LABELLA *et al.* 2020). In neurons, this isoform switch from normal ankyrin to Giant ankyrin at the correct time is critical to restrain juvenile patterns of neuronal development. The protein kinase A KIN-20 allows transcription to bypass the proximal polyA site and produce giant ankyrin. In *kin-20* mutants, giant ankyrin is not produced, GABA neurons develop abnormally, and mutant animals are severely uncoordinated. Hypomorphic alleles of several 3' mRNA cleavage complex genes were isolated in a genetic screen for mutants that suppress the *kin-20* Unc phenotype. These mutants disfavor the utilization of the proximal polyA site in *unc-44*, leading to the production of giant ankyrin. Likewise, in the hypertonic stress response, APA of a specific target via regulation of the 3' mRNA processing complex could be required for appropriate execution of this physiological response. In this respect, one possible APA target is *gpdh-1.* However, evidence from thousands of RNAseq datasets does not reveal evidence for APA of *gpdh-1* itself (STEBER *et al.* 2019) and genetic studies show that *gpdh-1* null alleles can still activate hypertonic adaptation (URSO *et al.* 2020). Instead, we hypothesize that 3' mRNA cleavage performs a similar function in the hypodermis and intestine to that in the neurons, where it regulates polyA site usage of a signaling gene that is an essential signaling component of the hypertonic stress response. Alternatively, the function of the

3' cleavage complex could regulate isoform switching for a suite of genes, such as extracellular matrix genes, whose collective function appears to be critical for the hypertonic stress response (ROHLFING *et al.* 2010; ROHLFING *et al.* 2011; DODD *et al.* 2018). Arguing against this second possibility is our observation that removal of the SYMK-1 protein in young adults after deposition of the ECM and immediately before exposure to hypertonicity is sufficient to block the hypertonic stress response. Defining the APA targets of 3' mRNA cleavage complex in the *C. elegans* hypodermis using RNAseq and evaluating their functional roles in the Nio phenotype represents an important future direction and will help to further distinguish between these and other models.

Subcellular localization could also play a major role in the regulation of mRNA cleavage. Both CPF-2 and SYMK-1 are expressed in all observable somatic and germline nuclei in *C. elegans*. We found that hypertonic stress causes both proteins to undergo reorganization into subnuclear foci. The function of these foci is unclear. Recently, hyperosmotic stress was found to result in the phase separation of the APA factor CPSF6 (JALIHAL *et al.* 2020), which leads to functional impairment of mRNA cleavage and polyadenylation. Whether or not this relocalization of the APA complex in *C. elegans* is related to its role in the Nio phenotype is not known. We found that introducing the G42E missense Nio allele into CPF-2 did not impact its ability to form subnuclear foci in response to hypertonicity or to colocalize with SYMK-1. Further studies will be needed to determine if hypertonic stress leads to functional impairment of transcriptional termination in *C. elegans* as it does in mammalian cells and whether or not large-scale termination events or target-specific APA contributes to the Nio phenotype.

In the same genetic screen that identified *cpf-2* and *symk-1*, we also identified null alleles in the O-GlcNAc transferase *ogt-1* (URSO *et al.* 2020). The discovery of all three genes in the same genetic screen suggests they might act together as part of the same signaling complex. However, our data suggest this may not be the case. First, *ogt-1* regulates *gpdh-1* expression via a post-transcriptional mechanism while *cpf-2* and *symk-1* function at the transcriptional level. Second, while both OGT-1 and CPF-2/SYMK-1 are nuclear proteins and form subnuclear foci in response to hypertonicity, these foci are spatially distinct. Despite these differences, there could be regulatory interactions between *ogt-1* and the 3' cleavage complex. For example, a recent study shows that the TPR domain of mammalian OGT interacts with the 3' cleavage complex components PCF11 (CFIIm complex) and CPSF1 (STEPHEN *et al.* 2021). Interestingly, it is the TPR domain, and not the catalytic activity, of OGT-1 that is required for the hypertonic stress response in *C. elegans* (URSO *et al.* 2020). Studies examining the role of *ogt-1* in the regulation of APA events will be needed to differentiate between these possibilities.

While the occurrence of APA has been known for several years, the regulatory mechanisms that determine which polyA site in a given gene will be utilized remains mysterious. Genetic approaches in organisms such as *C. elegans*, provide a powerful opportunity to study this highly conserved and essential complex in many dynamic, tissue-specific settings. The tools and insights developed in this study will play a major role in future studies aimed at understanding the physiologically relevant targets of 3' mRNA cleavage and alternative polyadenylation in the hypertonic stress response and investigating the mechanisms that drive polyA site switching in response to dynamic environmental changes.

Materials and methods

***C. elegans* strains and culture**: Strains were cultured on standard NGM media with *E.coli* OP50 bacteria at 20°C unless otherwise noted. Hypertonicity was induced by increased plate NaCl concentration to either 200 or 600 mM NaCl. For the auxin-induced degradation experiments, we included 0.5-1.0 mM Naphthaleneacetic Acid (K-NAA) in the NGM media prior to pouring plates. A list of strains used in this study can be found in Table 1.

Genetic methods: L4 stage *drIs4* animals (P_0) were mutagenized in 0.6 mM N-ethyl-N-nitrosourea (ENU) diluted in M9 for 4 hours at 20°C and Nio mutants were isolated as previously described (URSO *et al.* 2020). Backcrossing of both *nio-3(dr16)* and *nio-7(dr23)* to the wild type *drIs4* strain showed that both mutants were recessive. Trans-heterozygotes between *dr16* and *dr23* exhibited complementation. SNPs in both *dr16* and *dr23* were identified using whole genome resequencing and a Galaxy workflow (URSO *et al.* 2020). Candidate genes were tested using gene-specific RNAi in the *drIs4* background. RNAi was performed as described previously (URSO *et al.* 2020).

COPAS Biosort Acquisition and Analysis: Day one adults from a synchronized egg lay or hypochlorite preparation were seeded on 50 or 250 mM NaCl OP50 or the indicated RNAi NGM plates. After 18 hours, the GFP and RFP fluorescence intensity, TOF, and EXT of each animal was acquired with the COPAS Biosort. Events in which the RFP intensity of adult animals (TOF >400) was <20 (dead worms or other objects) were excluded from the analysis. The GFP fluorescence intensity of each animal was normalized to its RFP fluorescence intensity. To determine the fold induction of GFP for

327 each animal, each GFP/RFP was divided by the average GFP/RFP of that strain
328 exposed to 50 mM NaCl.
329
330 **CRISPR/Cas9 genomic editing**: For CRISPR editing, we injected purified and
331 assembled Cas9/gRNA/tracrRNA complexes with the purified repair template (all from
332 IDT) and the *rol-6* marker plasmid into the germlines of day 1 adult hermaphrodites.
333 Editing protocols primarily followed Ghanta et al with some modifications (GHANTA AND
334 MELLO 2020). We found that the high concentrations of nucleic acids frequently led to
335 precipitation of Cas9 complexes and needle clogging during injection. Reducing the
336 input levels of gRNA and tracer RNA to 20ng/µl and repair templates to 25 ng/µl (oligo
337 repair) or 10 ng/µl (PCR-based repair templates) prevented needle clogging and led to
338 similar numbers of editing events. Overall, 10-20 P0s were injected and 2-3 plates with
339 >10 rollers were selected for screening. Since CRISPR editing appears to occur
340 primarily in the distal germline while transgene formation occurs primarily in the proximal
341 germline, we screened 24 non-Rol F1 animals that were younger than the Rol animals
342 for editing events using edit-specific PCR approaches. We isolated homozygous edit-
343 positive animals from 2-3 independent heterozygous P0s. All edits were verified by DNA
344 sequencing. A list of all guide RNAs, repair template oligos/primers, and genotyping
345 primers can be found in Table 2.
346
347 **mRNA isolation, cDNA synthesis, qPCR, and polyA tail analysis**: Day one animals
348 were plated on 50 mM or 250 mM NaCl OP50 NGM plates for 24 hours. After 24 hours,
349 35 animals were picked into 50 µL Trizol for mRNA isolation. RNA isolation followed a
350 combined Trizol/RNeasy column purification method as previously described (ROHLFING
351 *et al.* 2010). cDNA was synthesized from 1 µg total RNA using the SuperScript VILO

352 Master Mix. SYBR Green master mix, 2.5 ng RNA, and the primers listed in Table 2
353 were used for each qPCR reaction. qPCR reactions were carried out using a BioRad
354 CFX qPCR machine. *act-2* primers were used as a control for all qPCR reactions. At
355 least three biological replicates of each qPCR reaction were carried with three technical
356 replicates per biological replicate. qPCR data was analyzed through ΔΔCt analysis with
357 all samples normalized to *act-2*. polyA tail length analysis was performed using the
358 Poly(A) Tail-Length Assay Kit (Thermofisher).
359
360 ***Symk-1-AID**** **alleles and auxin-induced degradation experiments**: *symk-1AID*GFP*
361 or *symk-1-AID*mNeonGreen* cassettes were PCR amplified from previously described
362 plasmids (ASHLEY *et al.* 2021) and used as the repair substrate for CRISPR/Cas9
363 injections into *TIR1; drIs4* strains. TIR1 strains were previously described (ASHLEY *et al.*
364 2021). AID* alleles of *symk-1* recapitulated the *symk-1* null phenotype (100% emb/larval
365 lethal) when gravid adults expressing TIR1 globally were placed on plates containing
366 either 0.5mM or 1.0mM K-NAA. For tissue-specific Nio experiments, AID* homozygotes
367 eggs were placed onto NGM plates containing 0.5mM or 1mM KAA (Sigma). L4 stage
368 animals were picked to new 1mM auxin plates and aged for 24 hours. Day 1 adults
369 were placed on either 50 mM NaCl NGM / auxin or 250 mM NaCl NGM/auxin plates for
370 18-24 hours. For temporal experiments, Day 1 adult *symk-1-AID** were placed on
371 0.5mM K-NAA for 4 hours prior to transfer. Animals were then imaged and the GFP and
372 RFP signals from the *drIs4* reporter were quantified on a COPAS Biosort.
373
374 **Microscopy**: For whole worm images, worms were anesthetized (10mM levamisole)
375 and manually arrayed on agar plates for fluorescence microscopy. Images were
376 collected on a Leica MZ16FA stereo dissecting scope with a DFC345 FX camera (Leica

Microsystems, Wetzlar, Germany). Images within an experiment were collected using the same exposure and magnification settings.

***kin-20* and *lin-15* suppression assays** – The *ox423* allele of *kin-20* was CRISPR edited into WT, *cpf-2(dr99)*, or *symk-1(dr88)*. Verified *kin-20* homozygotes in each background were placed on a clean NGM plate as a Day 1 adult. Thirty seconds of movement was video captured using a Leica M205 microscope and DFC camera at 15 frames per second. These data were analyzed for multiple kinetic and kinematic parameters using WormLab (MBF Biosciences).

For *lin-15* suppression, *cpf-2(dr99)* and *symk-1(dr88)* heterozygous males were crossed into *lin-15(n765ts)* at the permissive temperature (16ºC) using standard genetic crossing and genotyping methods. For unknown reasons, the *symk-1(dr88)* allele was synthetic lethal with *lin-15(n765ts)*, preventing further analysis. Animals were analyzed for the presence of a multivulval phenotype at the restrictive temperature (20ºC).

Statistical Analysis: Comparisons of means were analyzed with either a two-tailed Students t-test (2 groups) or ANOVA (3 or more groups) using the Dunnett's or Tukey's post-test analysis as indicated in GraphPad Prism 7 (GraphPad Software, Inc., La Jolla, CA). p-values of <0.05 were considered significant.

Data Availability Statement: Strains and plasmids are available upon request. The authors affirm that all data necessary for confirming the conclusions of the article are present within the article, figures, and tables.

Acknowledgements

We thank Maria Veroli Noguera, Ph.D. (Pitt) and Robert G. Kalb, M.D. (Northwestern) for critical reading and review of the manuscript prior to submission and Marco Mangone, Ph.D. (Arizona State University) for helpful discussions.

407 **Conflict of Interest Statement**

408 The authors have no conflicts of interests to declare

409

410 **Figure legends**

411 **Figure 1. *nio-3* and *nio-7* are caused by missense mutations in the**
412 **polyadenylation complex genes *cpf-2* and *symk-1*.** A) Protein domains found in
413 SYMK-1 and CPF-2. The location of each missense mutation is indicated. For *cpf-2*, we
414 used the available crystal structure of the APA complex to map the location of the
415 conserved G42 residue on the yeast homolog of *cpf-2*, Rna15 (PANCEVAC *et al.* 2010).
416 B) Overlayed transmitted light and GFP images of CRISPR-engineered animals carrying
417 missense Nio alleles of either *symk-1* or *cpf-2* exposed to either 50 or 250 mM NaCl for
418 18 hours. C) COPAS quantification of animals imaged in B. Bar graphs show the mean
419 ± S.D., with individual data points overlayed. D) Hypertonic adaptation of CRISPR Nio
420 alleles with or without a genomic DNA rescue transgene. Data are the mean ± S.D. of 4-
421 5 independent replicates of 10-20 worms per replicate.

422

423 **Figure 2. *cpf-2* and *symk-1* are required for hypertonic stress induced mRNA**
424 **expression.** qPCR of the *gpdh-1*, *gfp* (from the *drIs4* reporter), *hmit-1.1*, and *nlp-29*
425 mRNAs in wild type, *symk-1(dr88)*, and *cpf-2(dr99)* young adult animals exposed to 50
426 mM or 250 mM NaCl NGM. Data are the mean ± S.D. of 4 independent biological
427 replicates. Individual data points are plotted. ****- $p<0.0001$, ***-$p<0.001$, *-$p<0.05$, ns-
428 $p>0.05$, One-way ANOVA with Sidak multiple comparisons test.

429

430 **Figure 3. *symk-1* is required post-developmentally in the hypodermis and intestine**
431 **for the Nio phenotype.** A) Overlayed GFP and transmitted light images of *gpdh-1p::gfp*
432 expression following 24 hours of exposure to 50mM or 250mM NaCl. Animals express
433 TIR1 in the indicated tissues and were exposed to 1 mM K-NAA from the L1 stage. B)

434 COPAS Biosort quantification of GFP expression from animals shown in A. Data shown
435 are mean ± S.D. N=41-89 animals per sample. ****-p<0.0001, ns-p>0.05, One-way
436 ANOVA with Dunn's multiple comparison test. C) COPAS Biosort quantification of
437 animals with TIR1 expression in the hypodermis and intestine (*cpSi171*) exposed to 1
438 mM K-NAA for 0, 4, or 72 hours prior to exposure to 50mM or 250mM NaCl. Data
439 shown are mean ± S.D. N=35-61 animals per sample. ****-p<0.0001, ns-p>0.05.

440

441 **Figure 4. CPF-2 and SYMK-1 proteins colocalize into subnuclear puncta following**
442 **exposure to hypertonic stress.** Expression of CRISPR/Cas9-tagged alleles of *Tag-*
443 *RFP::cpf-2* (a) *symk-1::gfp* (b), and the merged image (c). d-f – higher resolution images
444 of hypodermal (hyp arrows) and germline (gl) nuclei revealing the non-nucleolar
445 nucleoplasmic concentration of tagged SYMK-1 and CPF-2 proteins. Dotted lines
446 delineate the boundaries of the germline. g-i – Exposure of animals to 600 mM NaCl for
447 1 hour leads to reorganization of SYMK-1 and CPF-2 into subnuclear foci, primarily in
448 the hypodermis. j-l – higher resolution of hypodermal nuclei with SYMK-1 and CPF-2
449 foci. m-o- higher resolution of hypodermal nuclei with SYMK-1 and CPF-2 carrying the
450 G42E Nio point mutation.

451

452 **Figure 5. *cpf-2* and *symk-1* suppress mutant phenotypes that depend on**
453 **alternative polyadenylation.** A) Transmitted light images of *lin-15* or *lin-15; cpf-2*
454 double mutants. Arrows in A point to multiple ectopic vulva which produces the
455 multivulval or Muv phenotype. B) Quantification of the % of Muv and nonMuv animals
456 from the indicated genotypes. ****-p<0.0001, Fishers exact test. N=102 animals for *lin-*
457 *15* and 120 animals for *cpf-2;lin-15*. C) Movement tracks for day 1 adult animals of the

indicated genotypes. Each color represents and individual track. D) Swim speed for day 1 adult animals of the indicated genotypes. Data shown are mean ± S.D for 10-24 animals per genotype. ****-p<0.0001, One way ANOVA with Dunn's multiple comparison test.

Figure 6. Inhibition of a subset of APA complex genes causes a Nio phenotype. A) Merged GFP and transmitted light images of *drIs4* animals fed either *empty vector(RNAi)* or RNAi against the indicated APA complex genes. Only images for animals exposed to 250 mM NaCl for 24 hours are shown for APA RNAi treatments. B) COPAS Biosort quantification of normalized GFP levels for each APA RNAi treatment following exposure to either 50 mM NaCl or 250 mM NaCl. Data shown are mean ± S.D. N=14-61 animals per sample. ****-p<0.0001, ns-p>0.05, One way ANOVA with Sidak's multiple comparison test.

Supplemental Figure legends

Figure S1. *cpf-2* and *symk-1* RNAi causes a Nio phenotype. *dris4* animals were fed *cpf-2* or *symk-1* RNAi from the L1 stage. Day 1 adult animals were exposed to 50 or 250 mM NaCl. GFP induction was quantified on a COPAS Biosort. Data shown are mean ± S.D. N=122-376 animals per sample. ****-p<0.0001, One way ANOVA with Sidak's multiple comparison test.

Figure S2. *nio-7(dr23)* and *nio-3(dr16)* Nio phenotypes are rescued by *symk-1* and *cpf-2* genomic DNA transgenes. A) *nio-7(dr23)* animals were injected with 20ng/µl of purified WRM0619bH10 containing the entirety of the *symk-1* genomic locus. Day 1

adult animals were exposed to 50 or 250 mM NaCl. GFP induction was quantified on a COPAS Biosort. Data shown are mean ± S.D. N=25-51 animals per sample. ****-p<0.0001, ns-p>0.05. One way ANOVA with Sidak's multiple comparison test. B) *nio-3(dr16)* animals were injected with 20ng/µl of a purified 5.1Kb PCR product containing the entirety of the *cpf-2* genomic locus. Day 1 adult animals were exposed to 50 or 250 mM NaCl. GFP induction was quantified on a COPAS Biosort. Data shown are mean ± S.D. N=25-51 animals per sample. ****-p<0.0001, ns-p>0.05. One way ANOVA with Sidak's multiple comparison test.

Figure S3 – A *symk-1::GFP::AID allele is functional rapidly degraded in the presence of 1mm K-NAA.** GFP images from animals carrying a globally expressed TIR1 transgene and homozygous CRISPR knock-in allele of the GFP::AID* cassette into the C-terminal region of symk-1. Following exposure to 1mM K-NAA, GFP expression is undetectable in all tissues after 3 hours.

Figures S4. The *symk-1::GFP::AID allele is functional.** A) Overlayed GFP and transmitted light images of drIs4 worms that are WT or homozygous for either the *symk-1(dr88)* or *symk-1::GFP::AID** insertion at the endogenous *symk-1* locus. Animals express TIR1 in the indicated tissues but were not exposed to auxin. B) COPAS Biosort quantification of GFP expression from animals shown in A. Data shown are mean ± S.D. N=71-130 animals per sample. ****-p<0.0001, One-way ANOVA with Dunn's multiple comparison test.

Fig S5 - CPF-2 and SYMK-1 hypertonic foci are distinct from OGT-1 foci. A-C) Hypodermal nuclei (arrows) in animals homozygous for a *TagRFP::cpf-2* (A) and *ogt-*

507 *1::GFP* alleles (B) form subnuclear foci upon exposure to 600 mM NaCl that fail to co-
508 localize (C). However, TagRFP::cpf-2 (D) and symk-1::GFP (E) exhibit complete
509 colocalization (F).
510
511 **Fig S6 - *cpf-2* and *symk-1* Nio mutants do not alter the RNA:DNA ratio.** 10 day 1
512 adult animals were placed in 12 µl PCR lysis buffer containing 1mg/ml proteinase K,
513 incubated at 60ºC for 1 hour, and then inactivated at 95ºC for 15 minutes. The resulting
514 lysate was used to measure DNA and RNA using the high sensitivity Qubit fluorimetry
515 assay.
516
517 **Fig S7 - *cpf-2* and *symk-1* do not alter polyA length/patterns for specific mRNAs.**
518 A) PCR amplification strategy for measuring polyA mRNA length. PCR reaction 1 shows
519 that the 5' primer is suitable for amplification. PCR reaction 2 amplifies from the 3' end of
520 the polyA tail. B)PCR reactions 1 and 2 for eight distinct mRNAs in the indicated genetic
521 background. 'No RT' – no reverse transcriptase added to cDNA synthesis reaction.
522
523 **Fig S8 - *cpf-2* and *symk-1* do not block *hsp-16p::GFP* induction by heat shock.** A)
524 Images of day 1 adults exposed to either control (20 ºC) or heat shock (3 hours of 35ºC
525 and 18 hours of recovery at 20ºC). B) COPAS Biosort quantification of GFP expression
526 from animals shown in A. Data shown are mean ± S.D, with individual data points
527 shown. N=33-61 animals per sample. ****-p<0.0001, One-way ANOVA with Dunn's
528 multiple comparison test.
529
530

References

Alt, F. W., A. L. Bothwell, M. Knapp, E. Siden, E. Mather *et al.*, 1980 Synthesis of secreted and membrane-bound immunoglobulin mu heavy chains is directed by mRNAs that differ at their 3' ends. Cell 20**:** 293-301.

Ashley, G. E., T. Duong, M. T. Levenson, M. A. Q. Martinez, L. C. Johnson *et al.*, 2021 An expanded auxin-inducible degron toolkit for Caenorhabditis elegans. Genetics 217.

Burkewitz, K., K. P. Choe, E. C. Lee, A. Deonarine and K. Strange, 2012 Characterization of the proteostasis roles of glycerol accumulation, protein degradation and protein synthesis during osmotic stress in C. elegans. PLoS One 7**:** e34153.

Calfon, M., H. Zeng, F. Urano, J. H. Till, S. R. Hubbard *et al.*, 2002 IRE1 couples endoplasmic reticulum load to secretory capacity by processing the XBP-1 mRNA. Nature 415**:** 92-96.

Chang, J. W., W. Zhang, H. S. Yeh, M. Park, C. Yao *et al.*, 2018 An integrative model for alternative polyadenylation, IntMAP, delineates mTOR-modulated endoplasmic reticulum stress response. Nucleic Acids Res 46**:** 5996-6008.

Chen, F., A. D. Chisholm and Y. Jin, 2017 Tissue-specific regulation of alternative polyadenylation represses expression of a neuronal ankyrin isoform in C. elegans epidermal development. Development 144**:** 698-707.

Clerici, M., M. Faini, R. Aebersold and M. Jinek, 2017 Structural insights into the assembly and polyA signal recognition mechanism of the human CPSF complex. Elife 6.

Clerici, M., M. Faini, L. M. Muckenfuss, R. Aebersold and M. Jinek, 2018 Structural basis of AAUAAA polyadenylation signal recognition by the human CPSF complex. Nat Struct Mol Biol 25**:** 135-138.

Cui, M., M. A. Allen, A. Larsen, M. Macmorris, M. Han *et al.*, 2008 Genes involved in pre-mRNA 3'-end formation and transcription termination revealed by a lin-15 operon Muv suppressor screen. Proc Natl Acad Sci U S A 105**:** 16665-16670.

Dodd, W., L. Tang, J. C. Lone, K. Wimberly, C. W. Wu *et al.*, 2018 A Damage Sensor Associated with the Cuticle Coordinates Three Core Environmental Stress Responses in Caenorhabditis elegans. Genetics 208**:** 1467-1482.

Ghanta, K. S., and C. C. Mello, 2020 Melting dsDNA Donor Molecules Greatly Improves Precision Genome Editing in Caenorhabditis elegans. Genetics 216**:** 643-650.

Ha, K. C. H., B. J. Blencowe and Q. Morris, 2018 QAPA: a new method for the systematic analysis of alternative polyadenylation from RNA-seq data. Genome Biol 19**:** 45.

Jalihal, A. P., S. Pitchiaya, L. Xiao, P. Bawa, X. Jiang *et al.*, 2020 Multivalent Proteins Rapidly and Reversibly Phase-Separate upon Osmotic Cell Volume Change. Mol Cell 79**:** 978-990 e975.

LaBella, M. L., E. J. Hujber, K. A. Moore, R. L. Rawson, S. A. Merrill *et al.*, 2020 Casein Kinase 1delta Stabilizes Mature Axons by Inhibiting Transcription Termination of Ankyrin. Dev Cell 52**:** 88-103 e106.

Lamitina, S. T., R. Morrison, G. W. Moeckel and K. Strange, 2004 Adaptation of the nematode Caenorhabditis elegans to extreme osmotic stress. Am J Physiol Cell Physiol 286**:** C785-791.

Lamitina, T., C. G. Huang and K. Strange, 2006 Genome-wide RNAi screening identifies protein damage as a regulator of osmoprotective gene expression. Proc Natl Acad Sci U S A 103**:** 12173-12178.

Mayr, C., and D. P. Bartel, 2009 Widespread shortening of 3'UTRs by alternative cleavage and polyadenylation activates oncogenes in cancer cells. Cell 138: 673-684.

Pancevac, C., D. C. Goldstone, A. Ramos and I. A. Taylor, 2010 Structure of the Rna15 RRM-RNA complex reveals the molecular basis of GU specificity in transcriptional 3'-end processing factors. Nucleic Acids Res 38: 3119-3132.

Pederiva, C., S. Bohm, A. Julner and M. Farnebo, 2016 Splicing controls the ubiquitin response during DNA double-strand break repair. Cell Death Differ 23: 1648-1657.

Pujol, N., S. Cypowyj, K. Ziegler, A. Millet, A. Astrain *et al.*, 2008 Distinct innate immune responses to infection and wounding in the C. elegans epidermis. Curr Biol 18: 481-489.

Rohlfing, A. K., Y. Miteva, S. Hannenhalli and T. Lamitina, 2010 Genetic and physiological activation of osmosensitive gene expression mimics transcriptional signatures of pathogen infection in C. elegans. PLoS One 5: e9010.

Rohlfing, A. K., Y. Miteva, L. Moronetti, L. He and T. Lamitina, 2011 The Caenorhabditis elegans mucin-like protein OSM-8 negatively regulates osmosensitive physiology via the transmembrane protein PTR-23. PLoS Genet 7: e1001267.

Ruepp, M. D., C. Schweingruber, N. Kleinschmidt and D. Schumperli, 2011 Interactions of CstF-64, CstF-77, and symplekin: implications on localisation and function. Mol Biol Cell 22: 91-104.

Shanbhag, N. M., I. U. Rafalska-Metcalf, C. Balane-Bolivar, S. M. Janicki and R. A. Greenberg, 2010 ATM-dependent chromatin changes silence transcription in cis to DNA double-strand breaks. Cell 141: 970-981.

Shi, Y., D. C. Di Giammartino, D. Taylor, A. Sarkeshik, W. J. Rice *et al.*, 2009 Molecular architecture of the human pre-mRNA 3' processing complex. Mol Cell 33: 365-376.

Steber, H. S., C. Gallante, S. O'Brien, P. L. Chiu and M. Mangone, 2019 The C. elegans 3' UTRome v2 resource for studying mRNA cleavage and polyadenylation, 3'-UTR biology, and miRNA targeting. Genome Res 29: 2104-2116.

Stephen, H. M., J. L. Praissman and L. Wells, 2021 Generation of an Interactome for the Tetratricopeptide Repeat Domain of O-GlcNAc Transferase Indicates a Role for the Enzyme in Intellectual Disability. J Proteome Res 20: 1229-1242.

Subramanian, A., M. Hall, H. Hou, M. Mufteev, B. Yu *et al.*, 2021 Alternative polyadenylation is a determinant of oncogenic Ras function. Sci Adv 7: eabh0562.

Urso, S., M. Comly, J. A. Hanover and T. Lamitina, 2020 The O-GlcNAc transferase OGT is a conserved and essential regulator of the cellular and organismal response to hypertonic stress. BioRxiv.

Wang, R., R. Nambiar, D. Zheng and B. Tian, 2018 PolyA_DB 3 catalogs cleavage and polyadenylation sites identified by deep sequencing in multiple genomes. Nucleic Acids Res 46: D315-D319.

Wheeler, J. M., and J. H. Thomas, 2006 Identification of a novel gene family involved in osmotic stress response in Caenorhabditis elegans. Genetics 174: 1327-1336.

Wimberly, K., and K. P. Choe, 2022 An extracellular matrix damage sensor signals through membrane-associated kinase DRL-1 to mediate cytoprotective responses in Caenorhabditis elegans. Genetics 220.

Yuan, F., W. Hankey, E. J. Wagner, W. Li and Q. Wang, 2021 Alternative polyadenylation of mRNA and its role in cancer. Genes Dis 8: 61-72.

630 Zheng, D., R. Wang, Q. Ding, T. Wang, B. Xie *et al.*, 2018 Cellular stress alters 3'UTR
631 landscape through alternative polyadenylation and isoform-specific degradation.
632 Nat Commun 9**:** 2268.

633

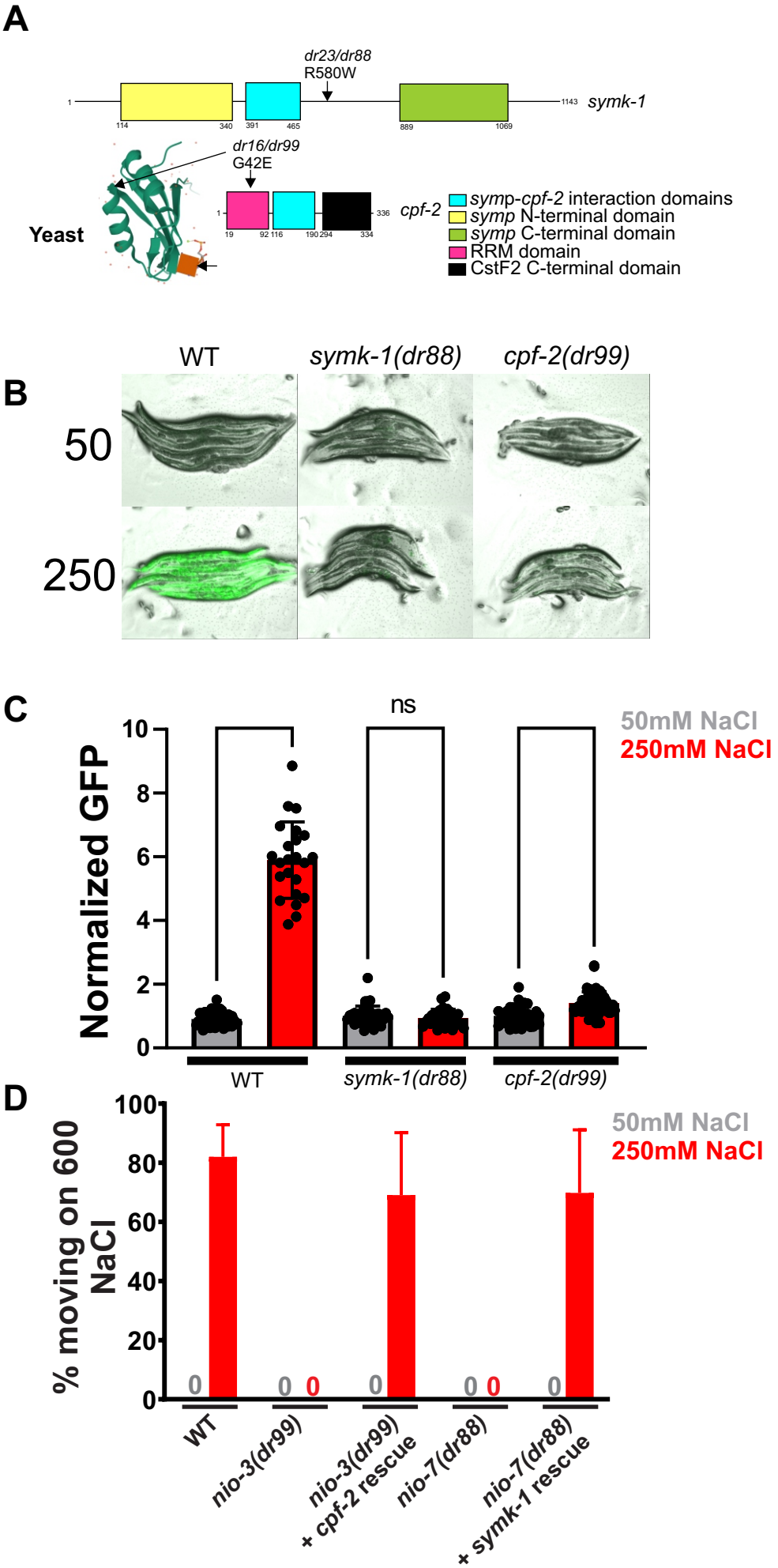
A
dr23/dr88
R580W
symk-1
dr16/dr99
G42E
Yeast
cpf-2
symp-cpf-2 interaction domains
symp N-terminal domain
symp C-terminal domain
RRM domain
CstF2 C-terminal domain
B
WT
symk-1(dr88)
cpf-2(dr99)
50
250
C
ns
50mM NaCl
250mM NaCl
Normalized GFP
WT
symk-1(dr88)
cpf-2(dr99)
D
% moving on 600 NaCl
50mM NaCl
250mM NaCl
WT
nio-3(dr99)
nio-3(dr99) + cpf-2 rescue
nio-7(dr88)
nio-7(dr88) + symk-1 rescue

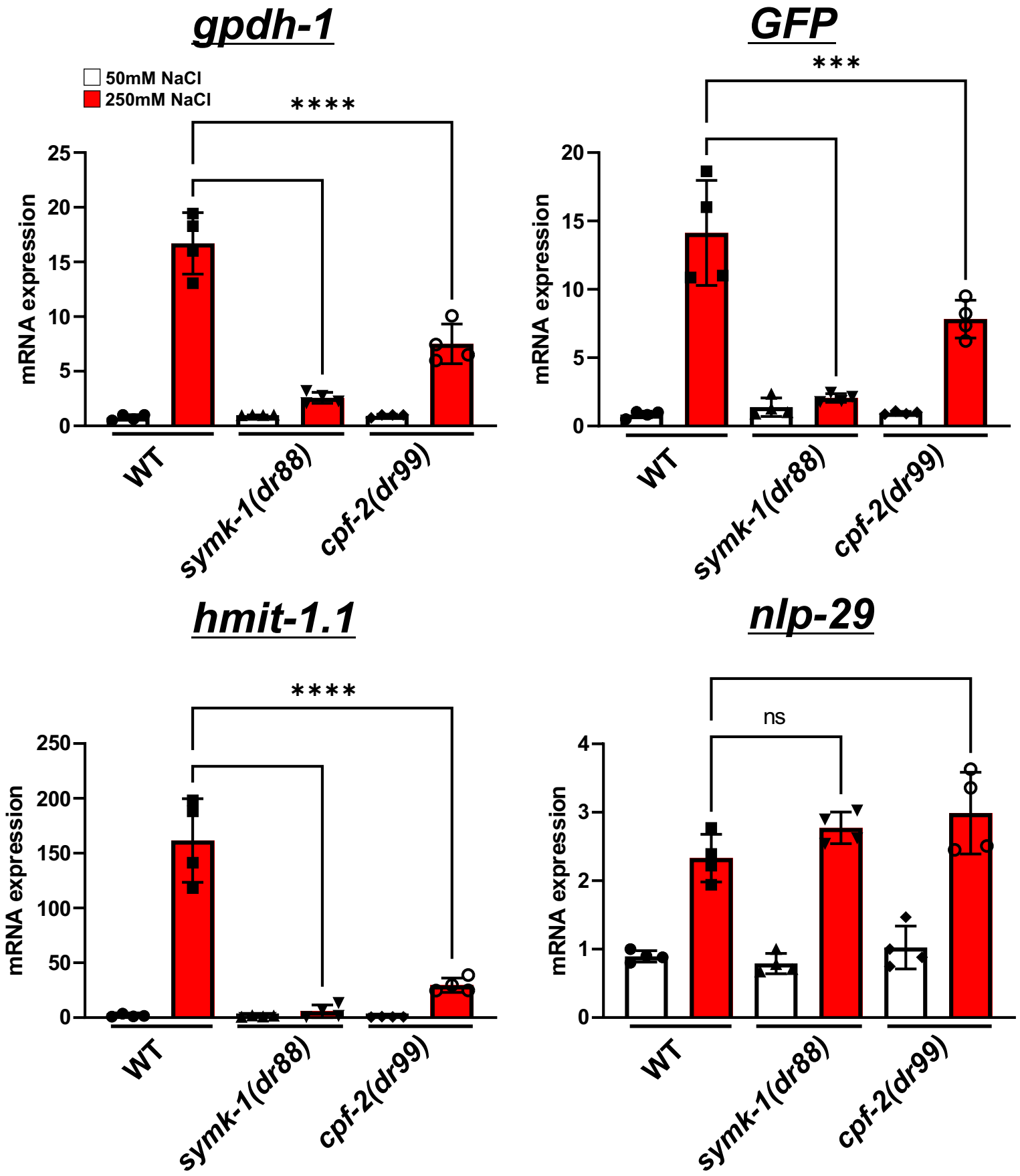
gpdh-1
50mM NaCl
250mM NaCl
****
mRNA expression
25
20
15
10
5
0
WT
symk-1(dr88)
cpf-2(dr99)
GFP
***
mRNA expression
20
15
10
5
0
WT
symk-1(dr88)
cpf-2(dr99)
hmit-1.1
****
mRNA expression
250
200
150
100
50
0
WT
symk-1(dr88)
cpf-2(dr99)
nlp-29
ns
mRNA expression
4
3
2
1
0
WT
symk-1(dr88)
cpf-2(dr99)

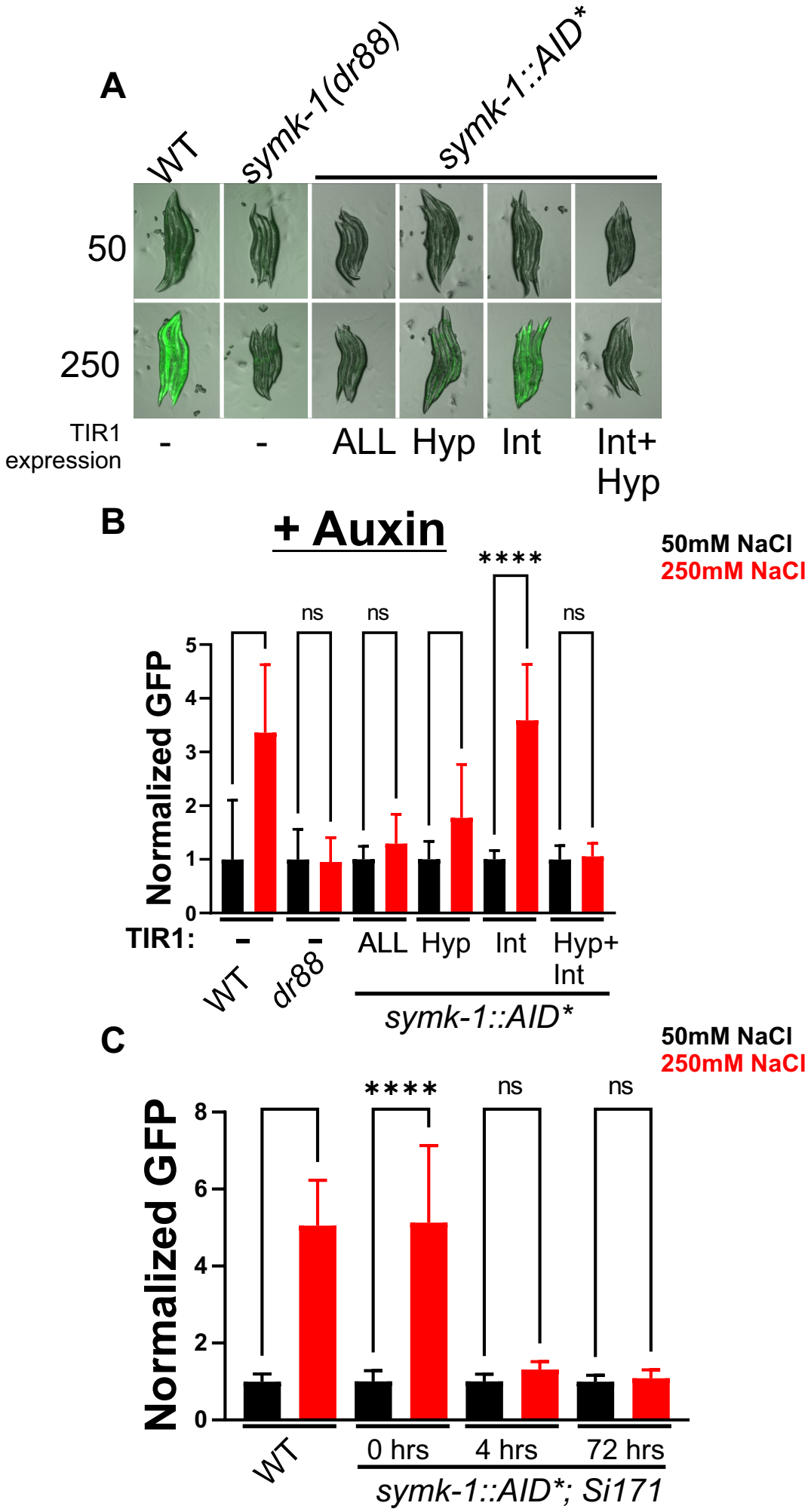
A
WT
symk-1(dr88)
symk-1::AID*
50
250
TIR1 expression
-
-
ALL
Hyp
Int
Int+ Hyp
B
+ Auxin
50mM NaCl
250mM NaCl
****
ns
ns
ns
Normalized GFP
0
1
2
3
4
5
TIR1:
-
-
ALL
Hyp
Int
Hyp+ Int
WT
dr88
symk-1::AID*
C
50mM NaCl
250mM NaCl
****
ns
ns
Normalized GFP
0
2
4
6
8
WT
0 hrs
4 hrs
72 hrs
symk-1::AID*; Si171

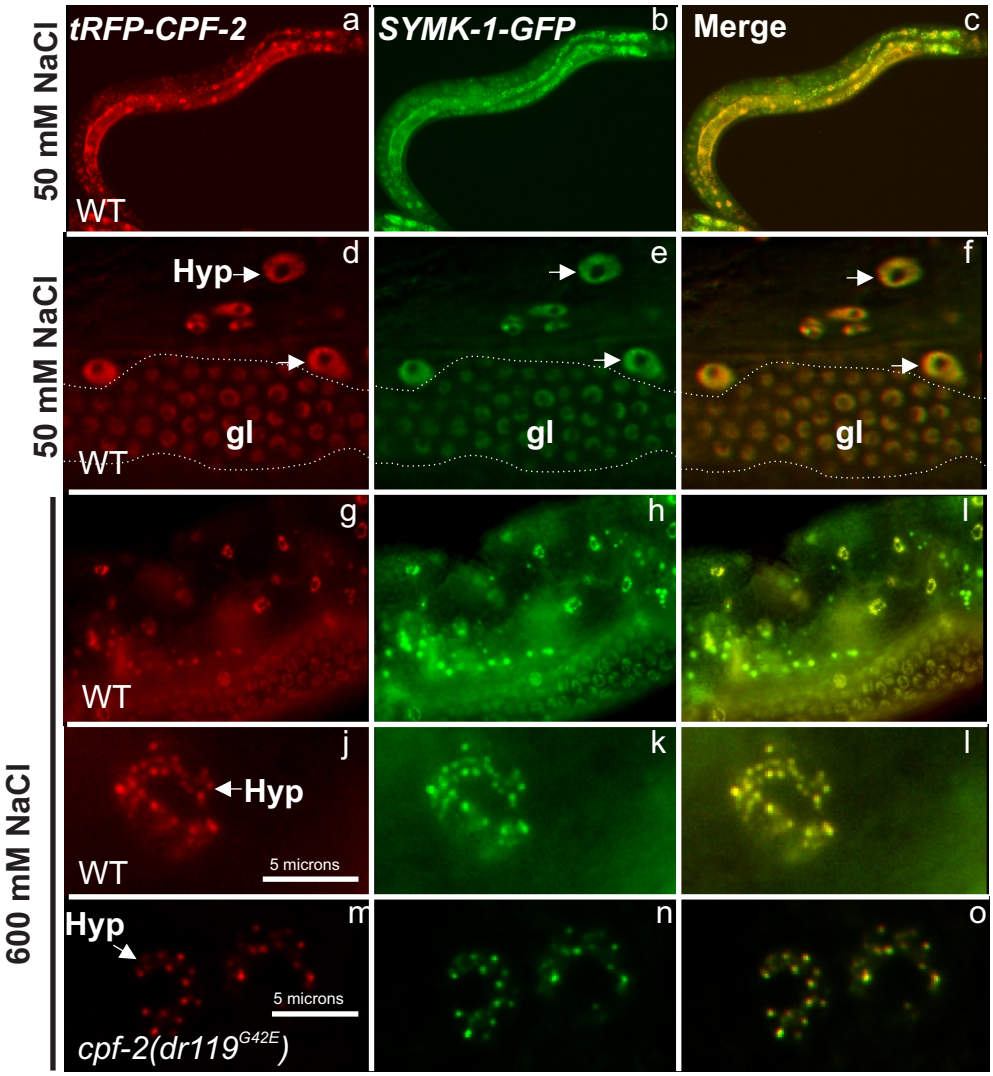
50 mM NaCl
tRFP-CPF-2
a
SYMK-1-GFP
b
Merge
c
WT
50 mM NaCl
Hyp
d
e
f
gl
gl
gl
WT
600 mM NaCl
g
h
i
WT
j
k
l
Hyp
WT
5 microns
Hyp
m
n
o
5 microns
cpf-2(dr119G42E)

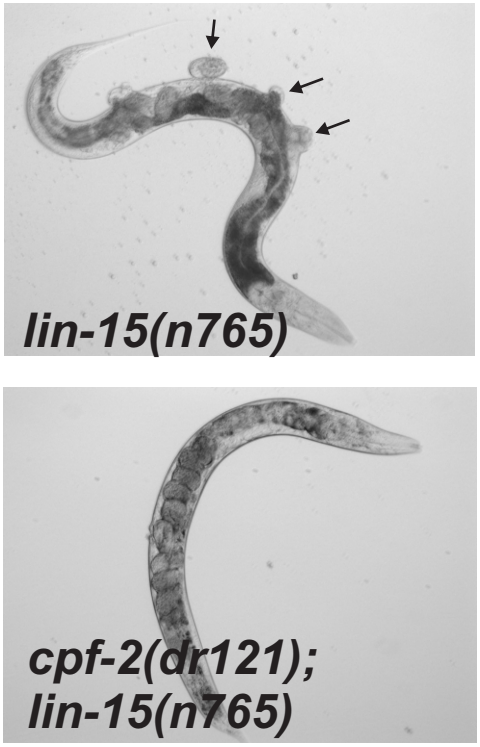
A
lin-15(n765)
cpf-2(dr121);
lin-15(n765)

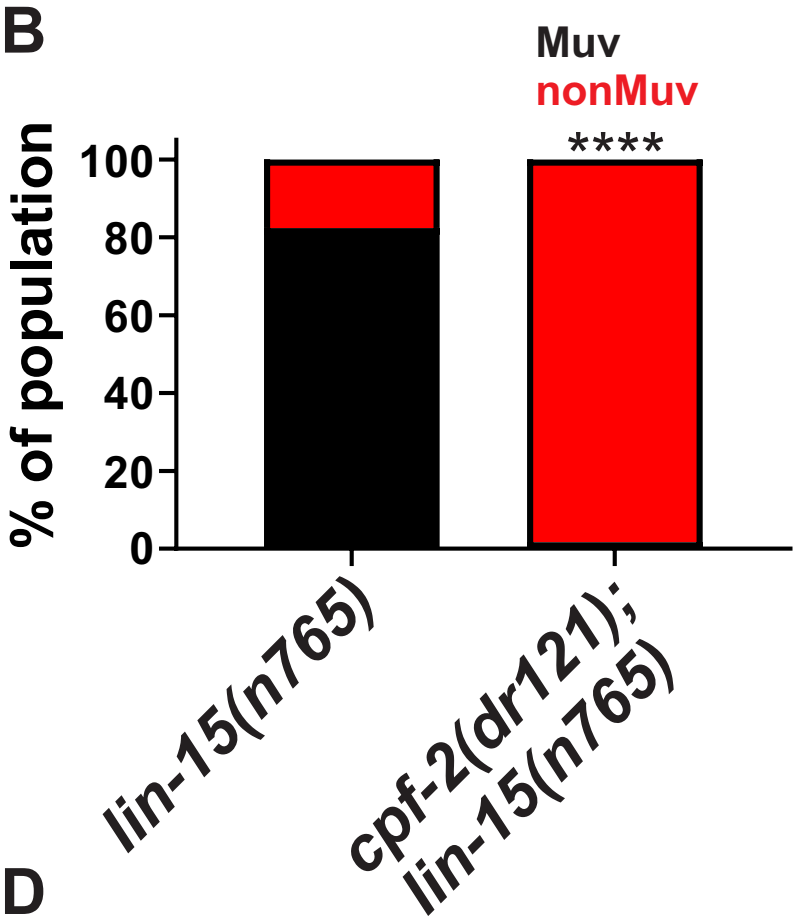
B
Muv
nonMuv
****
% of population
100
80
60
40
20
0
lin-15(n765)
cpf-2(dr121);
lin-15(n765)

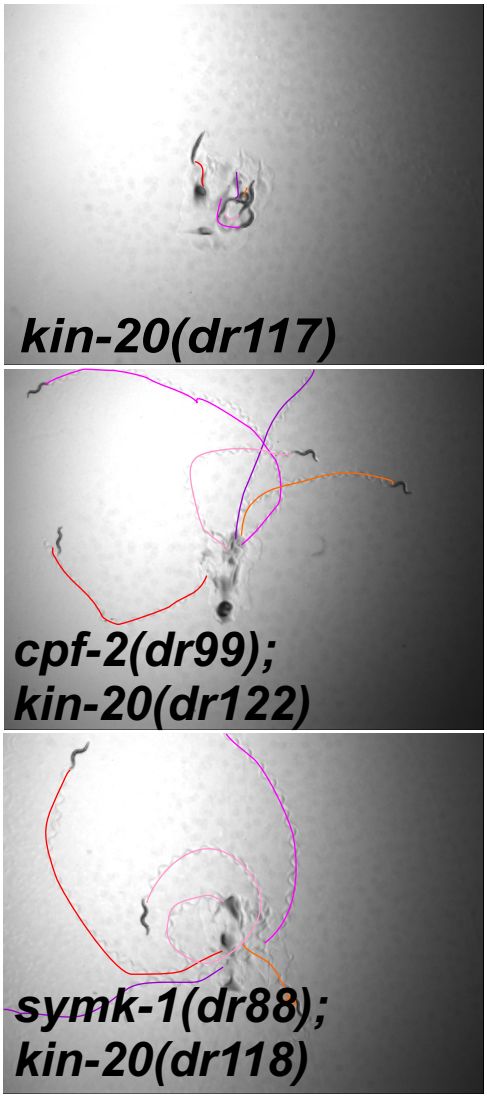
C
kin-20(dr117)
cpf-2(dr99);
kin-20(dr122)
symk-1(dr88);
kin-20(dr118)

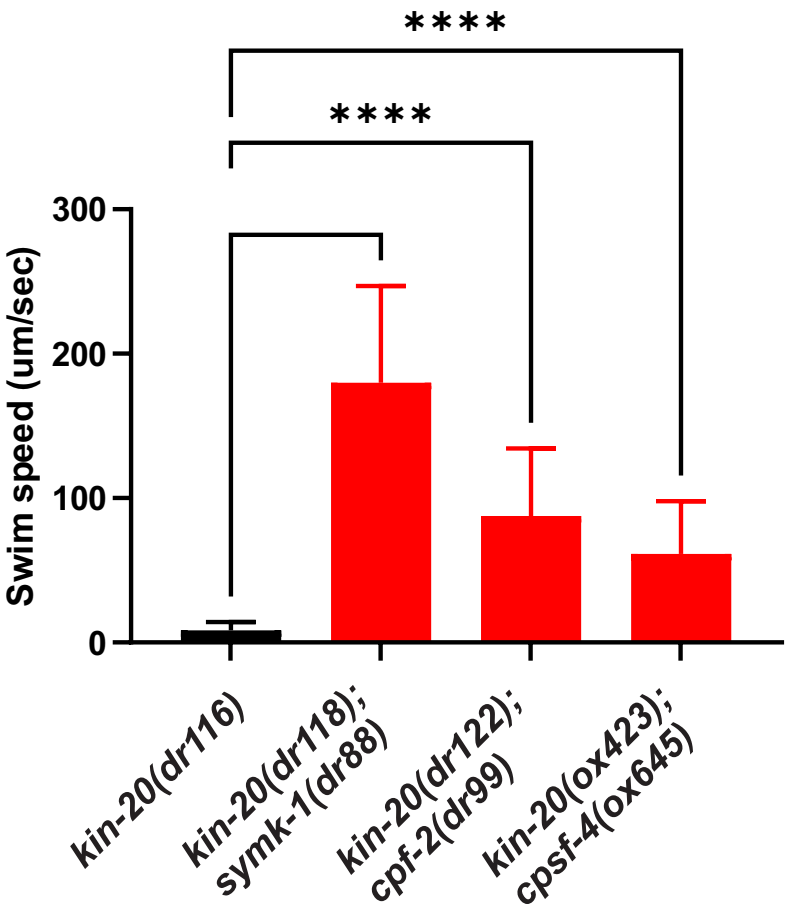
D
****
****
Swim speed (um/sec)
300
200
100
0
kin-20(dr116)
kin-20(dr118);
symk-1(dr88)
kin-20(dr122);
cpf-2(dr99)
kin-20(ox423);
cpsf-4(ox645)

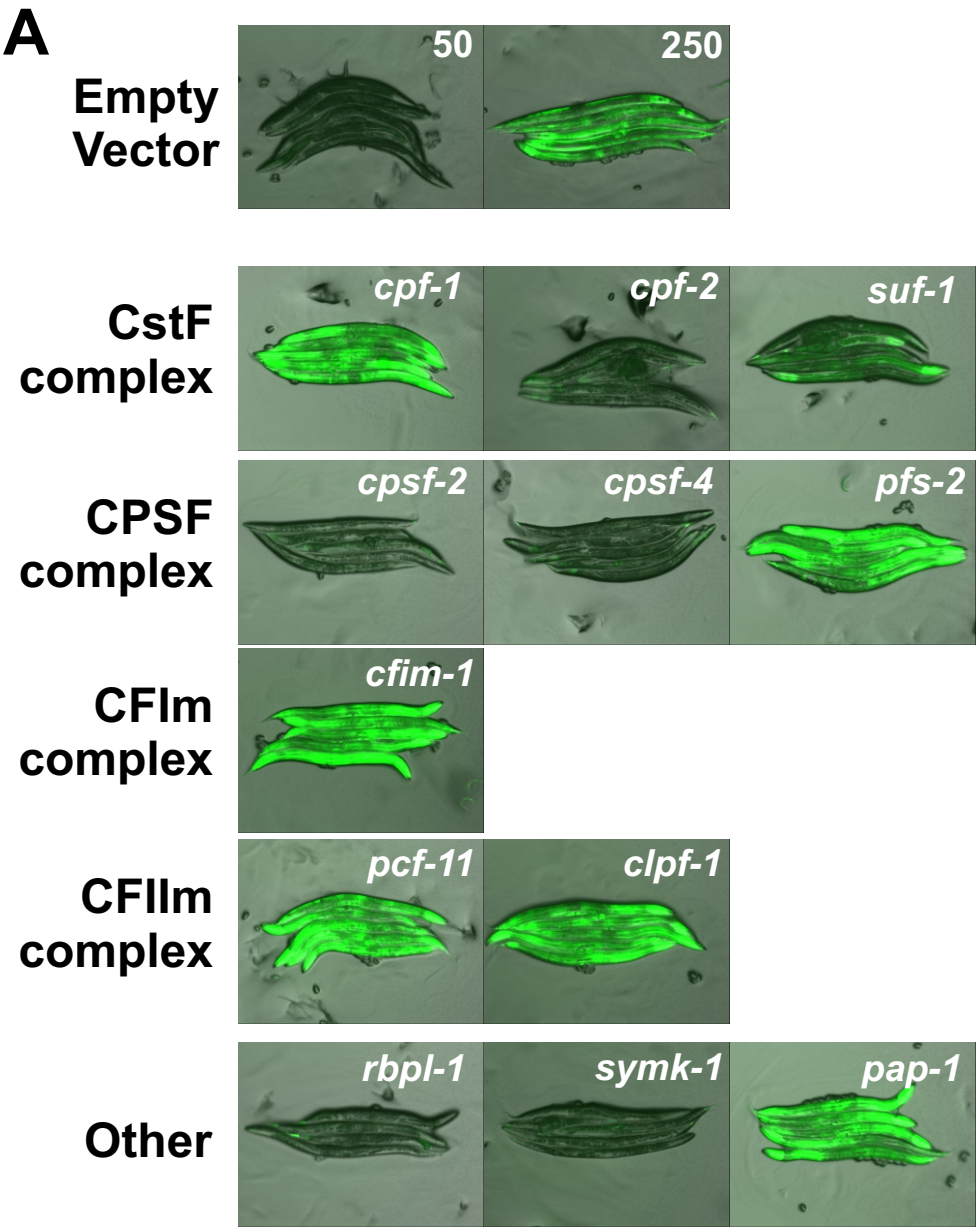
A
Empty Vector
50
250
CstF complex
cpf-1
cpf-2
suf-1
CPSF complex
cpsf-2
cpsf-4
pfs-2
CFIm complex
cfim-1
CFIIm complex
pcf-11
clpf-1
Other
rbpl-1
symk-1
pap-1

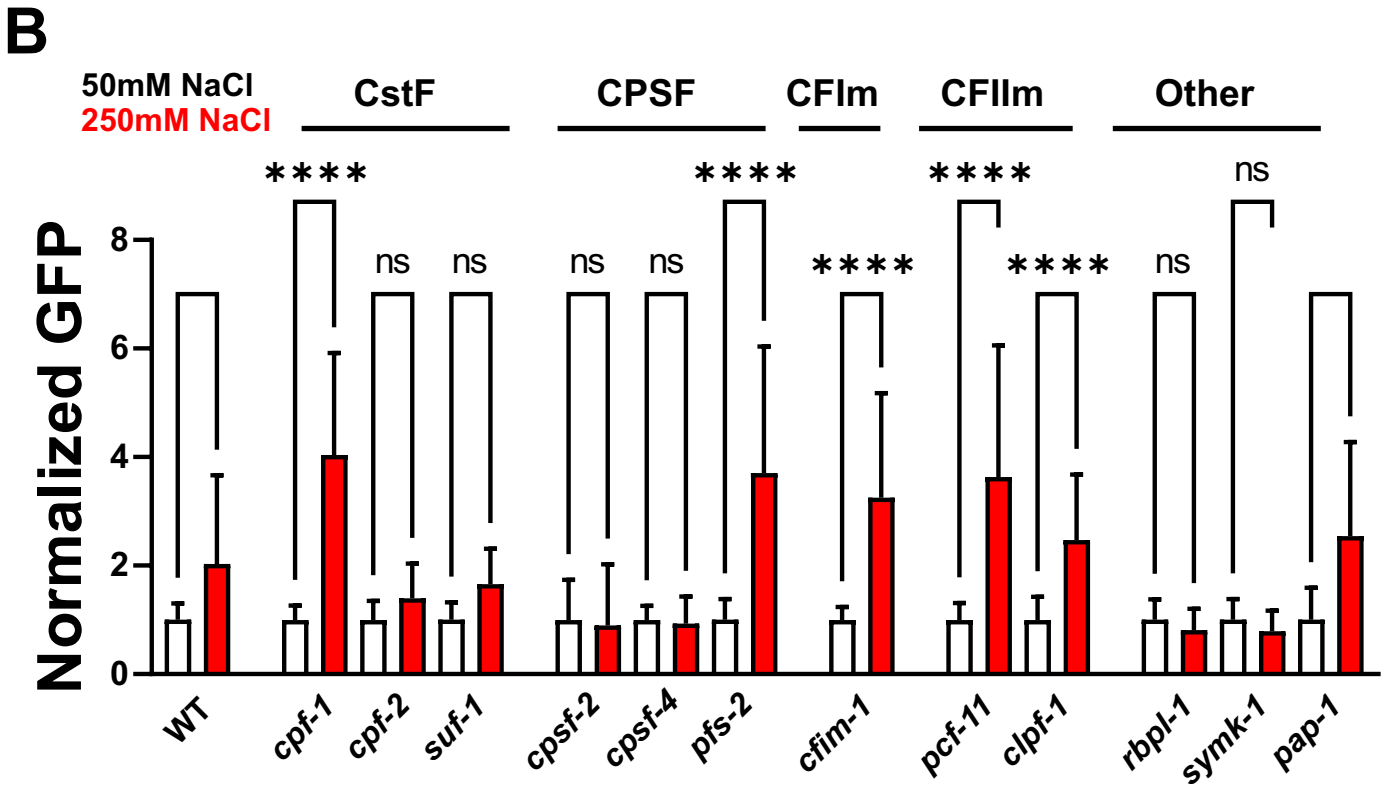
B
50mM NaCl
250mM NaCl
CstF
CPSF
CFIm
CFIIm
Other
Normalized GFP
0
2
4
6
8
****
ns
WT
cpf-1
cpf-2
suf-1
cpsf-2
cpsf-4
pfs-2
cfim-1
pcf-11
clpf-1
rbpl-1
symk-1
pap-1

Table 1. *C. elegans* strains

Strain	**Genotype**
OG119	*drIs4 (gpdh-1p::GFP; col-12p::dsRed2)*
OG975	*nio-3/cpf-2(dr16); drIs4*
OG996	*nio-7/symk-1(dr23); drIs4*
OG1137	*symk-1(dr88); drIs4*
OG1165	*cpf-2(dr99); drIs4*
OG1200	*kin-20(dr116)*
OG1202	*kin-20(dr118); symk-1(dr88)*
OG1207	*cpf-2(dr121); lin-15(n765ts)*
OG1209	*cpf-2(dr99); kin-20(dr122)*
OG1224	*wrdSi23* (eft-3p:TIR-1:F2A: mTAG BFP2:AID* NLS: tbb3'UTR); *drIs4*; *symk-1(dr127)* [*symk-1::AID*::GFP*]
OG1226	*reSi2* (col-10p:TIR-1:F2A: mTAG BFP2:AID* NLS: tbb3'UTR); *drIs4; symk-1 (dr129)* [AID* GFP CRISPR into *symk-1*]
OG1227	*reSi12* (ges-1p:TIR-1:F2A: mTAG BFP2:AID* NLS: tbb3'UTR); *drIs4; symk-1 (dr130)* [AID* GFP CRISPR into *symk-1*]
OG1241	*cpSi171* [vha-8p::TIR1::F2A::mTagBFP2::AID*::NLS::tbb-2 3'UTR]; *drIs4; symk-1(dr142)* [AID* mNeonGreen CRISPR into *symk-1*]
OG1142	*cpf-2(dr92)* [TagRFP CRISPR at N-terminus of CPF-2]
OG1144	*ogt-1(dr84); cpf-2(dr92)*
OG1194	*symk-1(dr111)* [GFP CRISPR just before NLS]
OG1195	*cpf-2(dr92); symk-1(dr112)* [GFP CRISPR just before NLS]
OG1203	*cpf-2(dr99); gpIs1*
OG1204	*symk-1(dr88); gpIs1*
OG1205	*cpf-2(dr92 dr119); symk-1(dr112)* [TagRFP::cpf-2 with G42E and symk-1::GFP]

Table 2. Primers used in this study

Primer	Primer sequence	Notes
OG592	TGCAGAGATTCCAGGAAACCAGG	gpdh-1 qPCR sense
OG593	CCCTTTTGTAGCTTGCCACGGAG	gpdh-1 qPCR antisense
OG596	GTAATGGATCCATCGCCAACAACTT	hmit-1.1 qPCR sense
OG597	GGTTAAGCCCGCGTATAGCCAAA	hmit-1.1 qPCR antisense
OG606	ggaggatatggaagaggatatggagga	nlp-29 qPCR sense
OG607	ccgtatcctccgtacattccacgtc	nlp-29 qPCR antisense
OG1342	tacctgttccatggccaacacttgtc	GFP qPCR sense
OG1343	CTTTCCTGTACATAACCTTCGGGC	GFP qPCR antisense
OG1720	ccgaagacacgattcgctccatt	cpf-2(dr16) sequencing fwr primer
OG1721	aacttcggcggtttgaatgtctg	cpf-2(dr16) sequencing rev primer
OG1722	cgataaagaagctgcggagatgt	symk-1(dr23) sequencing fwr primer
OG1723	gttcgagtagccttgatattgtg	symk-1(dr23) sequencing rev primer
OG1753	attttattctttccaattaaaatactgaaaaaaaggatccaggcagaaatgtgttgtcgatcaaaatggttcacgatcggg	ssDNA repair template for CRISPR conversion of WT to cpf-2/nio-3(dr16) Gly-->Glu
OG1756	gtggagcaaggttgatgtatcagaaattagttgtctggcttacaacgaggttt tgggaagattgtactccatttgaagaaaagttgat	ssDNA repair template for CRISPR conversion of symk-1 WT to dr23
OG1757	tccggctgacgactagattc	gRNA symk-1
OG1780	CAGGTTGAAAAATGATGTCC	gRNA for N-term CRISPR insertion of TagRFP into cpf-2
OG1781	aatttattcattttcaatttccaggttgaaaaatggtatccaagggagaagagttgatt	sense primer for TagRFP-cpf-2 N-term fusion (SP9 at 5' end)
OG1782	TTGCCCACTCCGGATGATTTGTATCCTCCGGACATGGCGCCGAATTCAGATCTCCTAGG	antisense primer for TagRFP-cpf-2 N-term fusion (SP9 at 5' end)
OG1783	gggtggagctagaggcaacgaatatg	tRFP-cpf-2 genotyping N-term
OG1784	GGATTCCTTGGGTGTGGTTGATGAAG	tRFP-cpf-2 genotyping N-term
OG1785	gcgggcgcgcagttttcgcaagtgtg	tRFP-cpf-2 genotyping N-term
OG1786	CGGGATCCGTACATGAAGGAGGTGGC	tRFP-cpf-2 genotyping N-term
OG1787	cacctaccgttccaagaagccagcc	tRFP-cpf-2 genotyping C-term
OG1788	CGAATTGCAACTTCGGCGGTTTGAATG	tRFP-cpf-2 genotyping C-term
OG1789	CAAGATGCCAGGAGTCTACTACGTC	tRFP-cpf-2 genotyping C-term
OG1790	GGAAATTCAATAAATCCGTATCCC	tRFP-cpf-2 genotyping C-term
OG1791	CGATCAAAATGGTTCACGAT	gRNA for CRISPR conversion of cpf-2 to dr16
OG1938	cttaattgtaataatttcagcgagaaaatcaaagaagagttgcatgatatgagtaaaggagaagaact	sense primer for symk-1-GFP template (SP9 modified at 5')
OG1939	AGTCGCTTATCTCGTTCACGATTTTCTCGTTCTTTTTTGTATAGTTCATCCATGC	antisense primer for symk-1-GFP template (SP9 modified at 5')
OG1940	ttcgaatcgttcgtcgcaaatc	symk-1 GFP screening primer
OG1941	TTCCTTTCCACTTTCGCGAGTTCG	symk-1-GFP screening primer
OG1942	GAAGATGTATCAACAATCGGATCG	symk-1 GFP screening primer
OG1943	GCGAGTTCGTTCCTTTTCTCTTTCC	symk-1-GFP screening primer
OG1944	GGGTAAGTTTTCCGTATGTTGCA	symk-1-GFP screening primer
OG1937	TTTCAGCGAGAAAATCAAAG	gRNA for symk-1 GFP
OG1953	aacatcaacatatcgcatat	kin-20 gRNA
OG1954	ttggactagcgaaacgctatcgtgatagcaaacattaacatatcgcatatcgc gaaaataagaatctaactggaactgcaagatacgc	kin-20(ox423) repair template with mutation
OG1955	gccggataacttttgatgggtct	kin-20 outer primer (sense)
OG1956	TGCAACTTCAAAAACATACCAATTC	kin-20 outer primer (antisense)
OG1957	gatgggtcttggaaagcgagg	kin-20 inner primer (sense)
OG1958	CCTCGATGAGTATTTATACTGGCG	kin-20 inner primer (antisense)
OG1959	GCATAAGGTGTTCACCGGGCACCAC	gpdh-1 3'UTR for polyA length assay
OG1960	GTTCATTCAAAATCAAAAATTGTACA	gpdh-1 3'UTR for polyA length assay
OG1983	AACCATGAAGATCAAGATCATCGC	act-2 3'UTR for polyA length assay
OG1984	CGGGGTGTGAAAATCCGTAAGGC	act-2 3'UTR for polyA length assay
OG1993	GTCTTCCTCCAGGGACCACGATCTG	rpl-18 sense - polyA length (spans exons 4/5)
OG1994	GACACATTTTTATTCGGCATGATTCG	rpl-18 3' UTR antisense - polyA length
OG1995	CAGATGAAGAAGGTTCTCTGCCTCTC	rpl-1 sense - polyA length (spans exons 2/3)
OG1996	CAACAATGTTTATTGAATAACAAAG	rpl-1 antisense - polyA length
OG1997	GGTTCATGATCAGGTTCTCGATGGAG	col-144 sense - polyA length (spans exons 1/2)
OG1998	GCAAACTTTATAATTGTGTGTTTGGAG	col-144 antisense - polyA length
OG1999	CAAGACGGACAACGTGGATCCGGAGC	col-144 sense - polyA length (in exon 2/use in case longer product doesn't work)
OG2000	GTCGCCGTTATCTCGGTGTGCGTCACTCTTCC	col-117 sense polyA length (spans exons 1/2)
OG2001	GTTGAATTTCTCATAACATTTAACGG	col-117 antisense - polyA length
OG2002	CCAAACGGAAACCCAGGAGCCCCAG	col-117 sense - polyA length (in exon 2/use in case longer product doesn't work)
OG2003	GGTTGAGGAAGCTGAGGAACTCGCCAAC	unc-54 sense - polyA length (spans exons 8/9)
OG2004	GTGTACACAGAACATTGTGTAGATTTTGGG	unc-54 antisense - polyA length
OG2005	CTCTTGCCCCATCAACCATGAAGATCAAG	act-3 sense - polyA length (spans exons 2/3)
OG2006	GATGGTCTTTTTGAATGGTCTCATGATCG	act-3 antisense - polyA length
OG2016	cttaattgtaataatttcagcgagaaaatcaaagaagagttgcatgatggtggcggtggatcgggaggaggagg	sense primer for amplifying GFP-AID* with symk-1 homology (SP9 at 5' end)
OG2017	AGTCGCTTATCTCGTTCACGATTTTCTCGTTCTTTGCCTCCGGACGATGCTCCTGAGGCTC	antisense primer for amplifying GFP-AID* with symk-1 homology (SP9 at 5' end)